Science of the Total Environment 792 (2021) 148452

Contents lists available at ScienceDirect

Science of the Total Environment

journal homepage: www.elsevier.com/locate/scitotenv

A novel glucose-based highly selective phosphate adsorbent

Hongxu Liang [a], Hongwei Zhang [a], Qiang Wang [a], Chenyang Xu [a], Zengchao Geng [a,*], Diao She [b,c,**], Xuguang Du [d]

[a] College of Natural Resources and Environment, Northwest A&F University, Yangling 712100, China
[b] State Key Laboratory of Soil Erosion and Dryland Farming on the Loess Plateau, Northwest A&F University, Yangling 712100, China
[c] Institute of Soil and Water Conservation, CAS&MWR, Yangling 712100, China
[d] Agricultural Technology Extension Station, Mian County, Hanzhong 724200, China

HIGHLIGHTS

- A kind of phosphate adsorption microporous carbon material (MCM) was prepared.
- MCM has a high effect on phosphate removal over a wide pH range (1.5–10).
- The phosphate removal rate of MCM was more than 99% in five kinds of water.
- The phosphate adsorption mechanism of MCM was investigated.
- MCM maintains >80% adsorption capacity after 20 regeneration cycles.

GRAPHICAL ABSTRACT

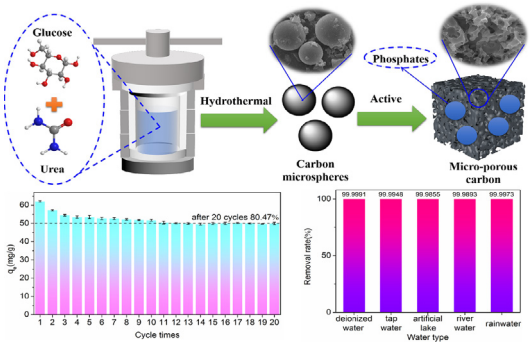

ARTICLE INFO

Article history:
Received 30 April 2021
Received in revised form 7 June 2021
Accepted 10 June 2021
Available online 16 June 2021

Editor: Huu Hao Ngo

Keywords:
Glucose
Phosphate
Adsorption
Microporous carbon material
High efficiency

ABSTRACT

Industrial wastewater discharge leads to serious eutrophication of water bodies, but most of the adsorbents are difficult to selectively remove phosphorus and are difficult to use multiple times, therefore, developing an efficient and reusable material for removal phosphate is extremely necessary. In this work, a kind of highly selective phosphate adsorbent, microporous carbon material (MCM), based on glucose was synthesized by hydrothermal and activation method. The MCM were characterized by SEM, XPS, BET, element analysis, et al. The phosphate adsorption mechanism of MCM were investigated by batch adsorption experiment and model calculation. Results showed that MCM had a high adsorption capacity for phosphate in a wide range of pH (1.5–10). Langmuir model and pseudo-second-order kinetic revealed that the process was endothermic and involved both physical and chemical adsorption. The main phosphate adsorption mechanisms of MCM are electrostatic attraction, ion complexation, hydrogen bonding, and physical adsorption. The ions competition simulation experiment indicated that the MCM was highly selective for phosphate removal. Furthermore, the phosphate adsorption tests were carried out on five kinds of water, and the removal rates were all above 99.98%. The 20 regenerative cycles experiment revealed that the MCM had high reusability. Therefore, this kind of novel glucose-based highly selective phosphate adsorbent with multi-cycle phosphorus removal performance can improve the eutrophication of water. This study provides a new idea for phosphate removal and expands the application range of glucose-based carbon materials.

1. Introduction

Phosphorus is a common elemental nutrient that can promote plant growth, increase grain yield, and ensure the normal operation of ecosystems, to relieve the agricultural pressure brought about by population

* Corresponding author.
** Correspondence to: D. She, State Key Laboratory of Soil Erosion and Dryland Farming on the Loess Plateau, Northwest A&F University, Yangling 712100, China.
E-mail addresses: gengzengchao@126.com (Z. Geng), diaoshe@ms.iswc.ac.cn (D. She).

https://doi.org/10.1016/j.scitotenv.2021.148452
0048-9697/

growth (Xiong et al., 2017; Zong et al., 2018; Turan et al., 2019). Phosphorus is important in water ecosystems, usually in the form of phosphate in water (Liu et al., 2019a; Zhang et al., 2018). Some studies have shown that phosphorus compounds can affect the availability of heavy metals and combine with plants to improve soil properties, so phosphorus is one of the most important elements (Rasool et al., 2021; Klammsteiner et al., 2020). However, due to the excessive use of chemical fertilizer and the discharge of industrial wastewater in recent years, the aquatic environment is destroyed by the enriched large amount of phosphorus (Carvalho et al., 2013; Fastner et al., 2015; Sonmez et al., 2016). One of the consequences of this is eutrophication, which causes proliferation of aquatic algae, resulting in reduction in oxygen in water and the death of organisms (Yin et al., 2018; Wang et al., 2020). In addition, residues of algae and aquatic organisms remain in water for a long time, resulting in a series of water pollution problems, such as bacterial breeding (Carpenter, 2008). Although countries have strictly limited the application of substances such as phosphorus-containing detergents—for example, the United States regulates the phosphorus content in industrial wastewater should at most 50 mg/L, but the phosphorus content in a large number of industrial wastewater sites is still far higher than the permitted value (Acelas et al., 2015; Zhang et al., 2019). Hence, it is urgent to reduce the phosphate content in water and minimize eutrophication.

Adsorption, and chemical precipitation, electrocoagulation, constructed wetlands, and other technologies are used to remove phosphate in water to solve the eutrophication and other pollution (Galvez-Cloutier et al., 2012; Hashim et al., 2019; Cui et al., 2020; Li et al., 2019). However, a comprehensive comparison of the cost and efficiency of these technologies shows that adsorption technology is low cost and highly efficient, so it is widespread used to treat water pollution (Zazycki et al., 2018; Saravanan et al., 2021; Deng et al., 2020). The common adsorption materials for phosphate and other pollution in water are MOFs (Liu et al., 2019a, 2019b;), clay (Unuabonah et al., 2017), carbohydrate (Turan, 2019), sludge (Buaisha et al., 2020), biomass (Meshkat et al., 2019), mineral (Bhatti et al., 2020), carbon-based materials (Turan et al., 2018a; Vikrant et al., 2018; Naeem et al., 2021) and metallic oxide (Zhang et al., 2019). Among them, the combination of biochar and other materials for pollution remediation has become a recent research hotspot (Turan et al., 2018b; Shahbaz et al., 2019; Turan, 2020; Zubair et al., 2021). Compared with other adsorption materials, carbon-based material has the features of low cost, easy preparation, and high yield, so they are widely used (Wang et al., 2020). However, at present, the adsorption of phosphate by most carbon materials is a long process, and their adsorption capacity and selective adsorption performance is low and they are difficult to use many times. In addition, most of the adsorbents are doped with metals such as La, Mg and Zr, which increases the risk of metal dissolution in water resulting in secondary contamination (Liu et al., 2019b; Bacelo et al., 2020). Hence, it is necessary to develop an no metal, high capacity, high selective performance, and recyclable adsorbent for the removal of phosphate. The MCM prepared from glucose in this study successfully solved these problems.

Glucose is the most abundant monosaccharide in almost all crops, and the large number of hydroxyl groups in its chemical structure is very beneficial to the adsorption process. In addition, glucose is easy to extract and very low cost, which makes it very suitable for the preparation of adsorbents. Hydrothermal (HT) synthesis is often used in the synthesis of carbon spheres from glucose and other sugars (Tong et al., 2019). The synthesized material have many reactive oxygen functional groups. The deficiencies of this technique are that the specific surface area of the synthesized carbon materials is very low, generally less than 100 m^2/g, and that agglomeration occur. These characteristics are not conducive to the adsorption reaction (Liang et al., 2020). Therefore, it is necessary to preserve the pore-making activation of this spherical carbon material to improve its specific surface area and adsorption performance. Since phosphorus generally exists as PO_4^{3-} in water, N can be doped in the material, leading to electrostatic attraction for NH_3^+ to promote phosphate adsorption, improve the performance of materials (Inagaki et al., 2018). Interestingly, hydrothermal reactions are often used for element doping. Therefore, carbon spheres containing N can be synthesized directly by a one-pot method. Using this modified carbon sphere material as the precursor and using activation technology to improve the surface morphology, carbon materials with a high surface area can be prepared. The previous work of our group also showed that the combination of hydrothermal and activation technology could prepare carbon materials with excellent adsorption performance for heavy metals. On the basis of our previous research, a novel glucose-based highly selective phosphate adsorbent was designed to removal of phosphate in water by mixing N element into MCM and improving the activation technology (activator and temperature, etc.).

In this work, carbon microspheres (CMSs) were prepared by a HT reaction using urea as the N source and mixing with glucose, followed by NaOH activation to prepare a microporous carbon material (MCM). The basic characteristics of MCM were explored through characterization techniques, and the adsorption ability of MCM for phosphate was investigated. By using a regeneration adsorption experiment, the adsorption performance of the regenerated MCM was investigated. The selective adsorption performance of MCM for phosphate was investigated by ion simulation and actual wastewater adsorption experiments. The mechanism of the adsorption reaction was explored by an adsorption model and calculating the thermodynamic parameters.

2. Material and method

All reagents were analytical grade, and specific information of the reagents is provided in Text S1 in the Supplement File.

2.1. Synthesis of CMSs

10 g glucose, 4 g urea and 150 mL deionized water were added to a 250 mL high-temperature reactor. A 3 cm magnetic rotor was used. The speed of the rotor was set at 500 r/min, the temperature was 185 °C, and the reaction time was 3.5 h. After the reaction, the sample was filtered through membrane to obtain CMSs.

2.2. Preparation of MCM

The prepared CMSs and NaOH were mixed according to a fixed ratio (CMSs:NaOH = 1:3), ground evenly with a mortar, immersed in deionized water, stirred for 24 h, and then dried by blast dryer. After drying, the sample is put into an atmosphere furnace. The temperature was set to 900 °C, the reaction time was 2 h for the activation treatment. After activated, the sample was washed with a large amount of deionized water to obtain the MCM. The flow chart for the synthesis of the MCM is shown in Fig. 1.

2.3. Material characterization method

Material characterization method and parameters supplemented in Text S2 with Supplement File.

2.4. Experiment of MCM adsorption of phosphate

The batch adsorption experiment used potassium dihydrogen phosphate to generate the phosphate solution. Fifty milliliters of phosphate solution was added to 100 ml plastic bottles, followed by the addition of 0.02 g MCM (0.4 g/L adsorbent). The adsorption experiment was carried out in a constant-temperature oscillation machine to explore the influence of different pH (1.5–10), different phosphate concentrations (50–200 mg/L), different temperatures (298–318 K) and different adsorption times (0.5–24 h) on the MCM adsorption of phosphate. The

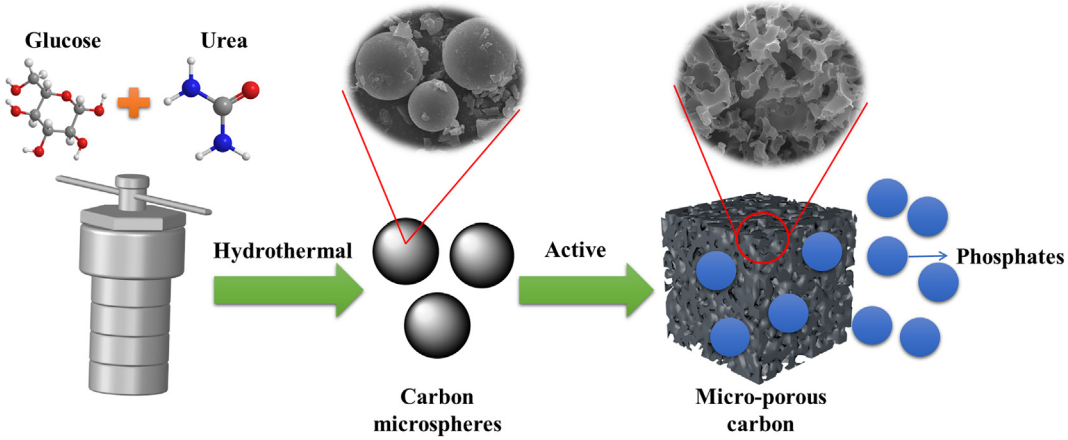

Fig. 1. The synthesis flow chart of MCM.

equation for phosphate adsorption capacity (q_e) after adsorption equilibrium is given by Eq. (1) (Oginni and Singh, 2021).

$$q_e = \frac{(C_1 - C_2)V}{m} \quad (1)$$

where C_1 and C_2 (mg/L) is the concentration of phosphate before and after adsorption; m (g) is the MCM mass; V (L) is the phosphate solution volume.

Origin 8.5 software was used to draw pictures and fit adsorption models such as isotherms, kinetics and intra-particle diffusion, and Excel 2020 was used to calculate thermodynamic parameters.

3. Results and discussions

3.1. CMSs and MCM characterization

3.1.1. Surface morphology and elemental analysis

The CMSs and MCM were characterized by SEM and TEM. The main structure of the material synthesized by the hydrothermal reaction was spherical, and the particle size was at the micron level, which indicated the successful synthesis of carbon microspheres (Fig. 2a). Moreover, the enlarged SEM image of the CMSs revealed a less porous structure than the MCM (Fig. 2b). Combined with the TEM results (Fig. 2c) and BET results (Table 1), it was found that the specific surface area of the CMSs

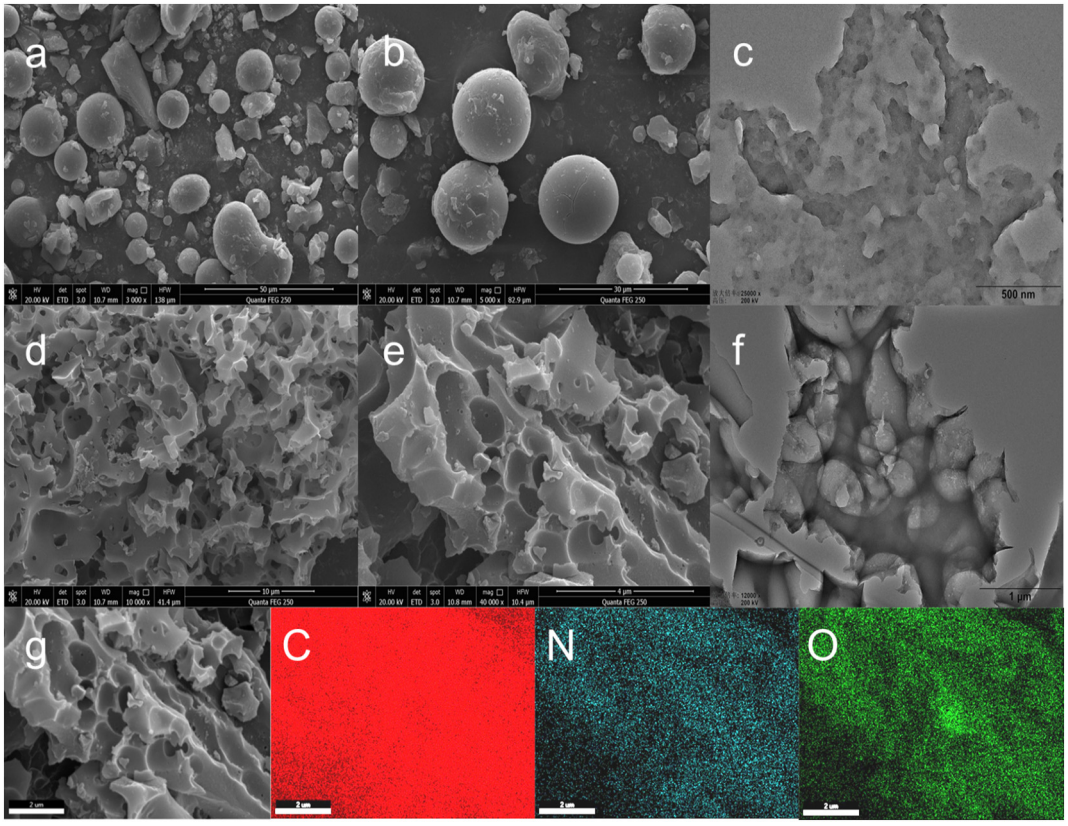

Fig. 2. The surface morphology and element distribution of CMSs and MCM: a and b is the SEM diagram of CMSs; c is the TEM diagram of CMSs; d and e is the SEM diagram of MCM; f is the TEM diagram of MCM; g is the SEM-EDX mapping diagram of MCM.

Table 1
The BET specific surface area and pore size distribution.

Material	Specific surface area (m^2/g)	Average pore size (nm)	Micropore volume (cm^3/g)
CMSs	1.30	17.61	4.6×10^{-5}
MCM	2045.14	1.93	0.15

was lower than that of the MCM, only 1.30 m^2/g. The SEM images of the MCM showed that surface of the material has a porous structure after activation treatment (Fig. 2d and e), and TEM confirmed that the pores of the MCM were well developed (Fig. 2f). The BET results showed (Table 1) that the main pore body of the material contained micropores, and the specific surface area was 2045.14 m^2/g, which proved that the MCM was a microporous carbon material with a high specific surface area. The SEM-EDX mapping images indicated that the material contains C, N and O (Fig. 2g), confirming that urea was involved in the reaction and that nitrogen-containing functional groups were successfully doped in the material. The elemental analysis results further prove that the content of N in the MCM was high, at 4.31% (Table 2), indicating that the MCM has more N functional groups than the CMSs, which is conducive for electrostatic attraction. In addition, the defects caused by N can capture pollutants, so the MCM has a very high adsorption performance.

3.1.2. Raman spectroscopy

To explore the structural properties of the materials, Raman spectroscopy was used (Liu et al., 2015). The Raman spectroscopy images show that the CMSs and MCM have D-band and G-band, which are characteristic of carbon materials, but the intensity of the two characteristic bands varied greatly (Fig. 3a and b). The D-band is located near 1350 cm^{-1} and is caused by the in-plane vibration of graphitic-C in the carbon material, while the G-band is located near 1580 cm^{-1} and is caused by disordered carbon in the material (Sun and Li, 2004). The higher the intensity of the D-band, the higher the degree of crystallization of the material; in contrast, the higher the intensity of the G-band, the more disordered and amorphous the lattice structure of the material. The intensity of the D-band of the CMSs is significantly greater than that of the G-band, which proves that the structure of the material is strong. The G-band of the MCM is almost equal to the D-band after the NaOH activation reaction, which confirms the increase in disordered carbon in the material. The MCM has an amorphous carbon structure. The increase in disordered carbon may be due to the etching of carbon materials by NaOH during activation, which destroys the original ordered lattice structure and leads to an increase in disordered amorphous carbon, thus enhancing the intensity of the characteristic G-band peak of the material (Liang et al., 2020). Furthermore, the incorporation of N also leads to a defective structure, which also confirms the results of the elemental analysis (Table 2).

3.1.3. XPS analysis

In this study, the chemical structure and elemental morphology of the CMSs and MCM were characterized by XPS. The XPS results showed that the characteristic peaks N1s and Na appeared in both CMSs and MCM but not the typical C1s and O1s characteristic peaks (Fig. 4), which demonstrated the successful hydrothermal reaction of urea with glucose. In addition, the presence of the Na peaks confirmed that SDS was involved in the reaction. Among the peaks, the intensity of the N1s peak of the MCM was lower than that of the CMSs, and the elemental analysis also confirmed that the content of N in the MCM was lower than that in the CMSs, which proved that the activation treatment destroyed N-containing functional groups. The C1s peak of the MCM was analyzed, and it was found that C mainly existed in four forms, namely, C—C/C═C/CH_x, C═N/—C—OR—, —COOR and C—N/C—OH (Wang et al., 2018). Analysis of the O1s peak of the MCM showed that O mainly existed in two forms, namely, —C—O— and C═O (Okpalugo et al., 2005). The N1s peak of the MCM was analyzed, and N mainly existed in three forms, namely, pyridinic-N, pyrrolic-N and graphitic-N (Wang et al., 2018). Pyridinic-N and pyrrolic-N have a good effect on improving the adsorption ability of materials, which proves that the adsorption ability of the MCM is relatively excellent, that the MCM can reduce the concentration of phosphate in water, and that the MCM can reduce environmental pollution (Liang et al., 2020).

Table 2
The element analysis table.

Material	N (%)	C (%)	H (%)	O (%)
CMSs	14.99	61.36	5.564	17.644
MCM	4.31	73.04	1.577	20.537

3.2. Adsorption experiment

3.2.1. Analysis of the factors that influence adsorption

The pH value can significantly affect the adsorption reaction. Because the pH of different environments is different, the Zeta potential of adsorbents in different environments is also different and the electrochemical characteristics of the surface of adsorbents also change, which results in electrostatic attraction or electrostatic repulsion of the target pollutant (Norouzi et al., 2018; Liang et al., 2019). In this work, the adsorption capacity of the MCM at pH range of 1.5–10 was tested, and it indicated that the adsorption ability reached a maximum near pH = 2 (Fig. 5a). When the pH was higher than 2, the q_e decreased with increasing pH, which may be caused by the different forms of phosphate at different pH values. From pH 3–9, phosphate existed in aqueous solution, mainly in the form of $H_2PO_4^-$ and HPO_4^{2-} (Zong et al., 2018), and the zeta potential test showed that the pH_{pzc} of the MCM near 4.7 (Fig. 5b). The charge of the surface was positive when the pH was less than 4.7 and negative when the pH was higher than 4.7, and as a result, when the pH was higher than 4.7, the material could produce electrostatic effects that repel phosphate, thus reducing the adsorption performance. In addition, as the pH increased, OH^- increased in solution, and this OH^- may compete with the phosphate anion. However, even when the pH was approximately 10, the adsorption ability decreased by only 10%, and compared with other adsorbents, MCM has good adsorption performance for phosphorus in a wide range of pH, which proves that the MCM has great practical application potential (Liu et al., 2020).

The concentration of phosphate has a great influence on adsorption because the higher the concentration of phosphate, the greater the differential concentration between the solution and MCM and the greater the potential energy of the solvent, which promotes the movement of phosphate into the adsorbent and thus improves the adsorption performance. In this work, the effect of the phosphate concentration from 50 to 200 mg/L on adsorption was tested, and it was found that the greater the phosphate concentration, the better the phosphate adsorption ability of MCM, which was in line with the prediction that the solvent potential energy would move phosphate into the MCM (Fig. 5c). In addition, the adsorption curves of different concentrations of phosphate had similar trends. After approximately 2 h, the adsorption reaction reached equilibrium, which indicates that the MCM can efficiently and quickly remove phosphate from water.

The adsorption reaction is usually endothermic or exothermic, so the temperature is highly important. In this study, the adsorption performance of MCM for phosphate under different temperature conditions was investigated. The test results showed that increasing the temperature increased the phosphate adsorption capacity of the MCM, which proved that increased temperature was beneficial to the phosphate adsorption onto the MCM (Fig. 5d). The increase in temperature led to the accelerated movement of phosphate molecules in the solution,

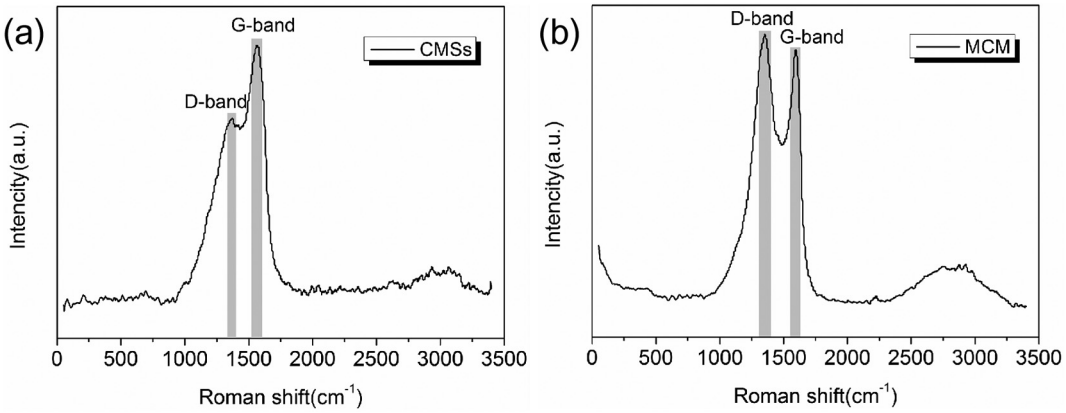

Fig. 3. The Raman spectrogram of CMSs and MCM: (a) is the Raman spectra of CMSs; (b) is the Raman spectra of MCM.

increasing the chance of contact with the MCM, which may be one of the reasons for the increase in adsorption ability. It is worth noting that in actual water treatment, due to the fermentation of microorganisms, the general sewage temperature is higher than room temperature. Therefore, the addition of the MCM will improve the adsorption of phosphate, which proves that the MCM is very suitable for the treatment of phosphate in actual wastewater and has high application potential.

3.2.2. Adsorption kinetics and adsorption diffusion model

In this work, pseudo-first-order (Eq. (2)) and pseudo-second-order (Eq. (3)) kinetic models were used to conduct a fitting analysis of the adsorption of phosphate on the MCM to explore the properties of the adsorption reaction (Zhang et al., 2013). The kinetic experiments were conducted at a phosphate concentration of 200 mg/g, and the MCM adsorption ability was tested at 30, 60, 120, 180, 240, 360, 480, 600 and 720 min.

$$q_t = q_e[1-\exp(-k_1 t)] \tag{2}$$

$$q_t = \frac{q_e^2 k_2 t}{(1+q_e k_2 t)} \tag{3}$$

where t (min) is time; k_1 and k_2 are the rate constants of the two kinetic models.

Kinetic curves show that there are roughly three stages of adsorption, namely, rapid adsorption, slow adsorption, and adsorption equilibrium stage (Liu et al., 2020). In addition, kinetic equation curves and related parameters show that after 120 min, the adsorption basically

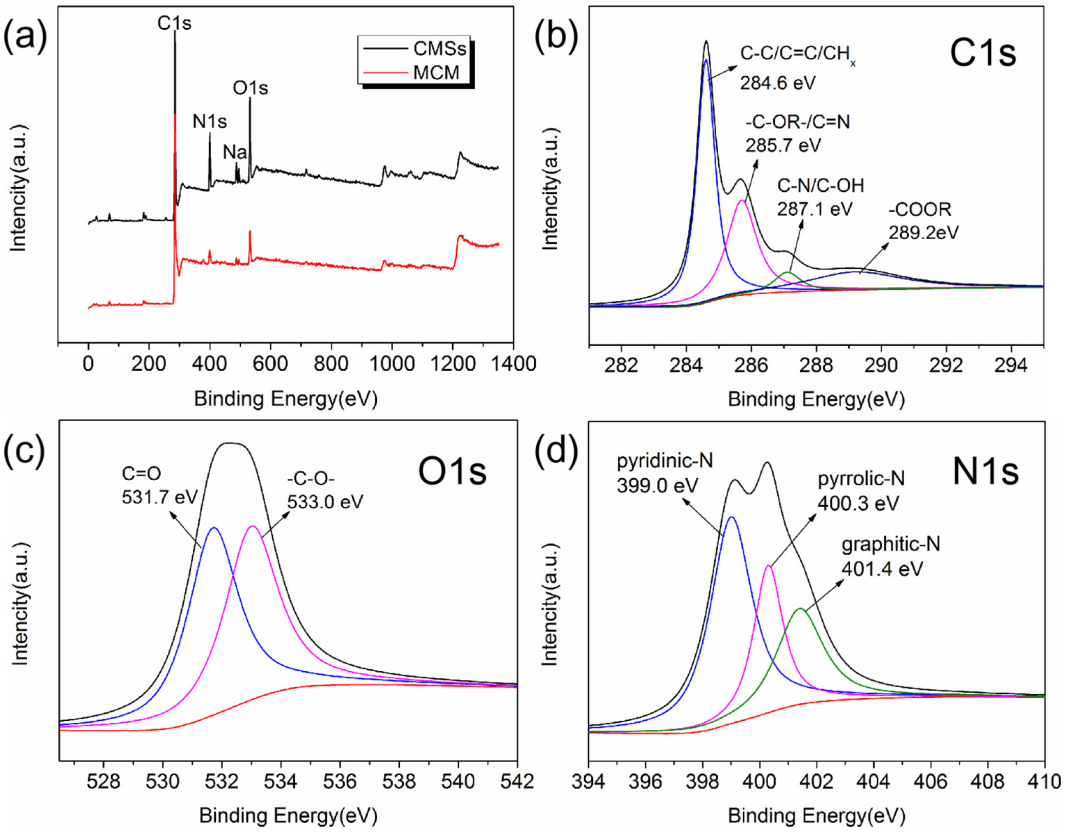

Fig. 4. The XPS diagram of CMSs and MCM: (a) is XPS diagram of CMSs and MCM; (b) is C1s diagram of MCM; (c) is O1s diagram of MCM; (d) is N1s diagram of MCM.

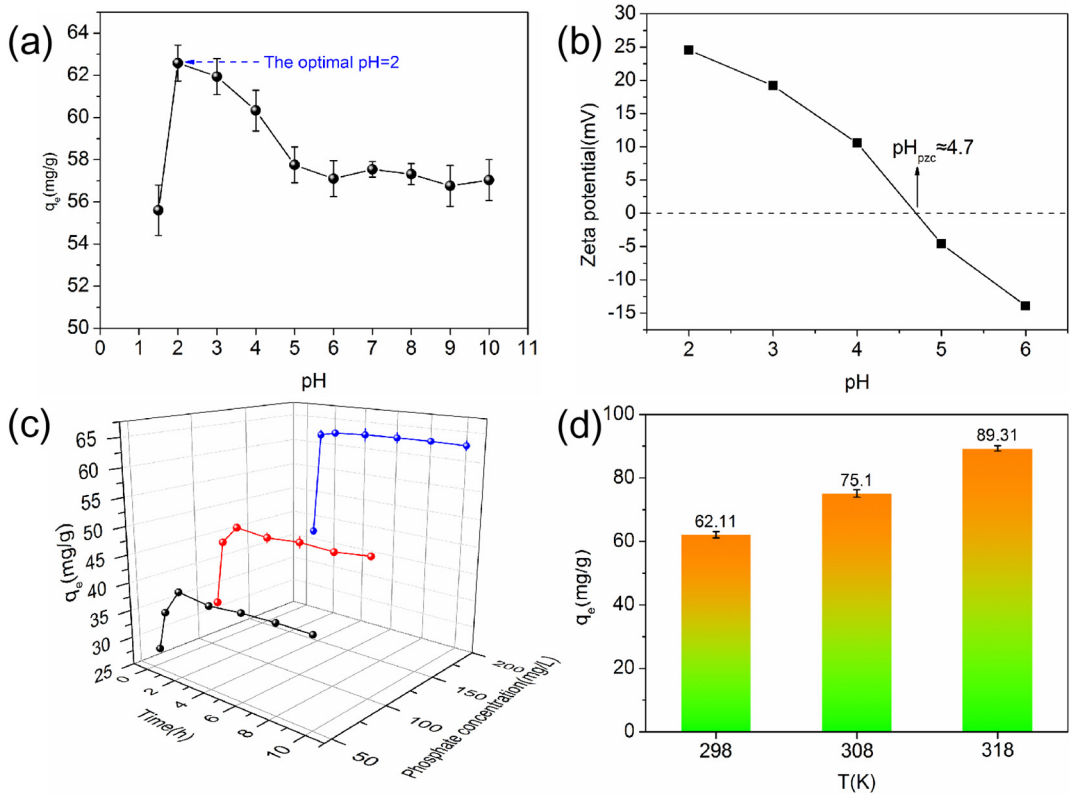

Fig. 5. The influence factor of adsorption process: (a) pH; (b) Zeta potential; (c) Cr(VI) concentrations; (d) Temperature.

reached equilibrium, which was consistent with the results in Fig. 5c. According to the Table 3, the two kinetic models accurately fit the adsorption reaction; although the R^2 value of pseudo-second-order kinetics model ($R^2 = 0.9973$) is slightly higher than that of the first-order kinetics model ($R^2 = 0.9952$), there is little difference. Furthermore, the equilibrium adsorption capacity predicted by the two kinetic models is close to the actual adsorption capacity. Therefore, both kinetic models can explain the phosphate adsorption process on the MCM, which also proves that the process is controlled by both physical adsorption and chemical adsorption, and the proportion of chemical adsorption may be slightly higher than that of physical adsorption (Liang et al., 2019). Due to the hydrothermal reaction and doping effect, the surface of MCM contains a large number of oxygen and nitrogen functional groups, which also leads to the generation of chemisorption.

On the basis of the kinetic results, this study further explored the adsorption process by using the intraparticle diffusion model (Eq. (4)) and Boyd diffusion model (Eqs. (5)–(7)) to analyze the main controlling factors of the phosphate adsorption by the MCM (Ketelle and Boyd, 1947).

$$q_t = K_{id} t^{0.5} + C \tag{4}$$

$$F = 1 - \left(\frac{\pi^2}{6}\right) exp\left(-B_t\right) \tag{5}$$

$$F = \frac{q_t}{q_e} \tag{6}$$

$$B_t = -0.4977 - ln\left(1 - F\right) \tag{7}$$

where t is time; K_{id} is the rate constant; and F is a mathematical function of B_t.

The adsorption curves of phosphate at different concentrations (50, 100, 200 mg/g) were fitted using the intraparticle diffusion model (Fig. 6b and Table 4). The after 120 min, the adsorption reaction basically reached equilibrium, which further confirmed the results in Fig. 5c and the results of the kinetics model (Fig. 6a). According to the parameters of the fitted equation (Table 4), the model does not reach a value of zero. Therefore, MCM adsorption of phosphate is controlled by many factors, such as surface adsorption, intra-particle diffusion and mass transfer (Wu et al., 2014; Liu et al., 2020). There are three stages of phosphate adsorption on MCM. The first stage is the 0–60 min, when the adsorption speed is extremely fast, so the value of the model parameter $K_{id,1}$ is also higher than that in other stages. This is because the adsorption of phosphate on the MCM is just beginning. The surface and internal adsorption sites of the MCM are not occupied by phosphate, and the difference between the concentrations of the MCM and phosphate in the solution is very large, generating a potential difference that drives phosphate molecules toward the MCM; therefore, with the increase of phosphate concentration in the solution, the potential difference will increase, leading to the increase of adsorption rate, and the different values of $K_{id,1}$ in Table 4 confirm the results. In the first 60 min, the surface adsorption sites are not occupied, so the main controlling factor is surface film diffusion. The second stage of adsorption occurs from 60 to 120 min. At this time, the adsorption rate decreases, and the $K_{id,2}$ value decreases because the adsorption site is occupied gradually (Liang et al., 2019). With the progress of adsorption, the differential concentration between the MCM and the solution decreases, and the driving force of potential energy decreases accordingly, so the adsorption rate begins to decrease. In this stage, because the surface adsorption sites are occupied, phosphate molecules gradually move

Table 3
The adsorption kinetic parameters.

Model name	Model related parameters
Pseudo-first-order	$k_1 = 3.38 \times 10^{-2}$, $q_e = 62.13$, $R^2 = 0.9952$
Pseudo-second-order	$k_2 = 9.63 \times 10^{-4}$, $q_e = 65.20$, $R^2 = 0.9973$

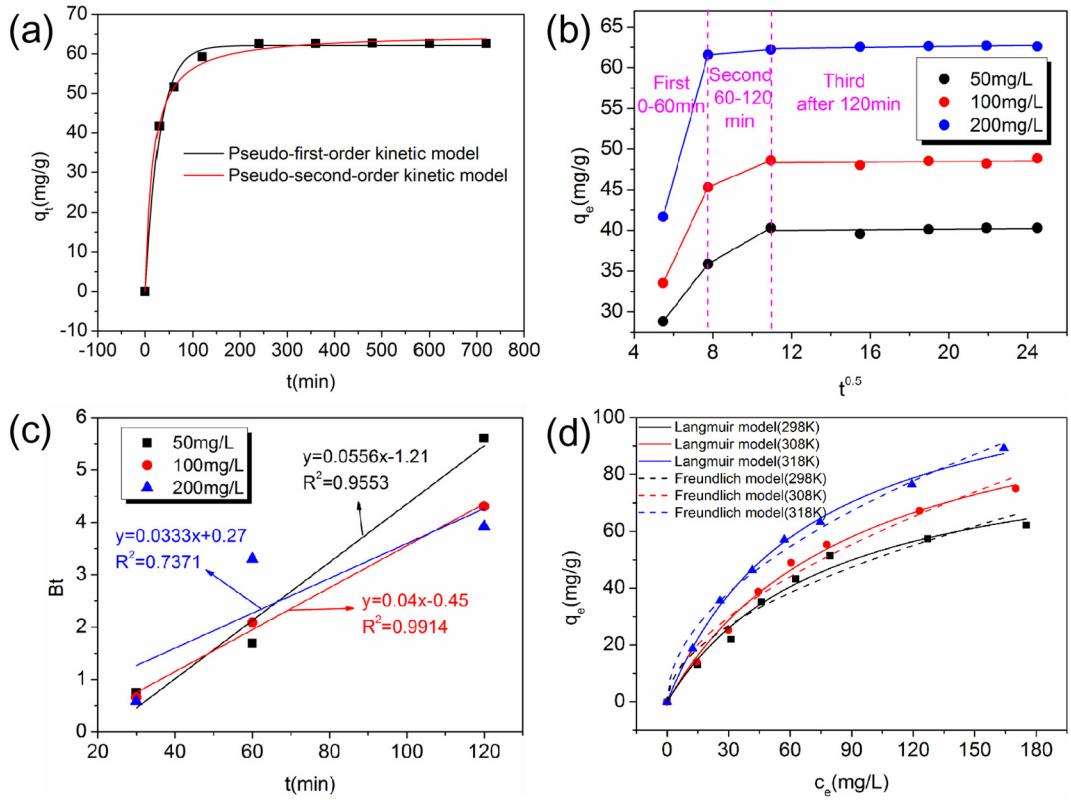

Fig. 6. Adsorption models of MCM: (a) is adsorption kinetics model; (b) is intraparticle diffusion model; (c) is linear fitting between Bt and t; (d) is adsorption isotherm model.

from the surface of the MCM to the internal adsorption sites. The controlling factors in this stage are surface film diffusion and intraparticle diffusion. In addition, because the adsorption rate of the second stage is much lower than that of the first stage, it is proved that intraparticle diffusion is the limiting factor for MCM to adsorb phosphate (Gupta and Ghosh, 2009; Jian et al., 2015; Liu et al., 2019a, 2019b). In the third stage of adsorption, the adsorption reaction reaches final equilibrium, the adsorption and desorption reach dynamic equilibrium, and the adsorption capacity does not change greatly.

The Boyd diffusion model was used to investigate the MCM adsorption of different concentrations of phosphate (50–200 mg/L). The results indicated that the Boyd model fit the adsorption process well (Fig. 6c). In addition, the straight line of the model fitting showed that the intercept of the fitting line is not zero, which confirmed that the adsorption is controlled by multiple factors (Liang et al., 2017). This finding also validates the results of the adsorption intraparticle diffusion model and adsorption kinetic, phosphate adsorption on MCM is controlled by multiple factors, and physical and chemical adsorption coexist. The reason that the adsorption is controlled by many factors may be caused by the irregular morphology and three-dimensional pore structure of MCM, which can also explain that intra-particle diffusion is the rate-limiting step of the whole adsorption process (Liang et al., 2021).

3.2.3. Adsorption isotherms

To further elucidate the phosphate adsorption properties on the MCM and explore the mechanism of the process, isotherm experiments were conducted to determine the phosphate adsorption by the MCM at three temperatures (298, 308, 318 K), and the adsorption data was fitted by the Langmuir (Eq. (8)) and the Freundlich model (Eq. (9)).

$$q_e = \frac{K_L q_{max} c_e}{1 + K_L c_e} \tag{8}$$

$$q_e = K_F c_e^{\frac{1}{n}} \tag{9}$$

where K_L and K_F are the constants of the model.

The adsorption trend of phosphate on the MCM is closer to the Langmuir isotherm, which indicates that the adsorption of phosphate by the MCM is closer to uniform monolayer adsorption and that the Freundlich isotherm, which represents multilayer adsorption, does not accurately describe this adsorption process (Fig. 6d and Table 5). The Langmuir isotherm indicated that the q_{max} of phosphate on the MCM was 92.79–123.73 mg/g (298 K–308 K), which is higher than that of most materials in the world (Table 6) (Haddad et al., 2018; Cui et al., 2016; Liu et al., 2019a, 2019b; Liu et al., 2018; Zong et al., 2013; Liu et al.,

Table 4
The parameters of intraparticle diffusion model.

Initial concentration of phosphate (mg/g)	$K_{id,1}$ (mg/g·min$^{0.5}$)	C_1	$K_{id,2}$ (mg/g·min$^{0.5}$)	C_2
50	3.11	11.80	1.39	25.12
100	5.19	5.10	1.03	37.34
200	8.78	−6.45	0.20	60.02

Table 5
The parameters of isothermal adsorption model.

T (K)	$q_{max,exp}$ (mg/g)	Langmuir model			Freundlich model		
		q_{max} (mg/g)	b (L/mg)	R^2	K_f	n	R^2
298	62.11	92.79	1.29×10^{-2}	0.9816	4.58	1.93	0.9481
308	75.10	118.39	1.07×10^{-2}	0.9937	4.35	1.77	0.9722
318	89.31	123.73	1.46×10^{-2}	0.9974	6.80	1.97	0.9890

Table 6
The performance comparison of other materials.

Material	pH	q_{max} (mg/g)	Reference documentation
Magnesium-pretreated biochar	5.2	66.7	Haddad et al., 2018
Magnesium-alginate/chitosan modified biochar	3.0	46.56	Cui et al., 2016
Magnetic zirconium-based metal–organic frameworks	3.0	16.95	Liu et al., 2019a, 2019b
MFC@La(OH)3	3.0	45.45	Liu et al., 2018
Zr-loaded graphite oxide	3.0	16.5	Zong et al., 2013
Hydroxyl–iron–lanthanum doped activated carbon fiber	–	29.44	Liu et al., 2013
Glucose and urea	2.0	123.73	This study

2013). In addition, MCM does not contain precious elements while many other adsorbents are loaded, which reduces the risk of secondary contamination due to metal adsorbents dissolving in water (Feng et al., 2017; Bui et al., 2021; Shan et al., 2021). Fig. 6d shows that the higher the temperature, the higher the phosphate q_{max} of MCM, which confirms the result in Fig. 5d and indicates that increasing temperature can promote the adsorption of phosphate on the MCM.

3.2.4. Thermodynamic calculation of adsorption

In this study, after determination of the adsorption isotherm parameters, the changes of adsorption free energy, heat and entropy were calculated using the thermodynamic formula Eqs. (10)–(12), and the adsorption mechanism was analyzed (Huang et al., 2014).

$$\Delta G^{\circ} = -RTlnK_a \tag{10}$$

$$\Delta G^{\circ} = \Delta H^{\circ} - T\Delta S^{\circ} \tag{11}$$

$$ln\,K_a = \frac{\Delta S^{\circ}}{R} - \frac{\Delta H^{\circ}}{RT} \tag{12}$$

where T (K) is the temperature in Kelvin and R is Avogadro's constant.

The results of the thermodynamic calculations are shown in Table 7. The Gibbs free energy calculated at different temperatures is negative, confirming that the adsorption of phosphate on the MCM is spontaneous. In addition, the absolute value of the Gibbs free energy increases gradually with increasing temperature, which indicates that the reaction is easy, confirming the conclusion that temperature promotes adsorption, as shown in the diagram and isotherm (Liang et al., 2018). The calculated adsorption heat is positive, which proves that adsorption is endothermic, which exactly explains why temperature is favorable for adsorption, this result is consistent with most studies (Feng et al., 2017; Liu et al., 2020). Therefore, adsorption of phosphate on MCM is spontaneous and endothermic, and it occurs precisely because the endothermic reaction accelerates molecular movement and increases disorder, which lead to an increase in adsorption entropy.

3.3. Adsorption-desorption regeneration experiment

In this work, a 1 M NaOH solution was used to desorb phosphate to conduct 20 adsorption-desorption regeneration cycles on the MCM (Fig. 7). The experimental results showed that in adsorption-desorption cycles 1–3, the phosphate adsorption performance of the

Table 7
The thermodynamic parameters for the adsorption of MCM.

T (K)	K_a (L/mol)	ΔG° (kJ/mol)	ΔH° (kJ/mol)	ΔS° (kJ/(K/mol))
298	399.51	−14.84	46.628	0.065
308	331.38	−14.86		
318	452.16	−16.16		

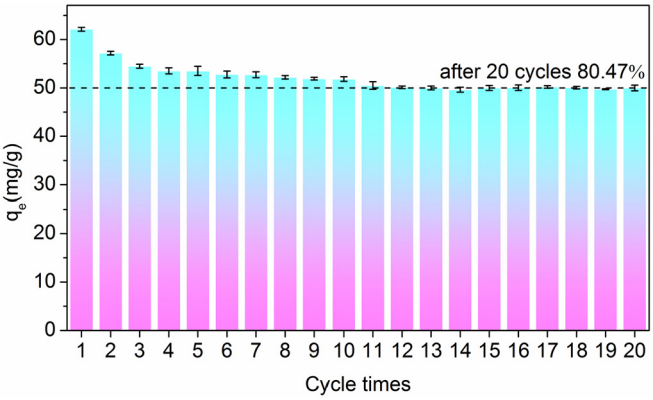

Fig. 7. The regenerative adsorption performance of MCM.

MCM decreased rapidly, while in cycles 3–10, the adsorption performance declined slowly. In cycles 11–20, the adsorption performance basically did not change, and during this cycle, the adsorption capacity was approximately 80.47% of the initial adsorption capacity. Therefore, the MCM is an excellent adsorption material for phosphate removal that can be recycled and has the potential for large-scale practical application.

To explore the mechanism for decreased adsorption performance of the material during the adsorption-desorption cycle, SEM and elemental analysis were performed on the initial material and the material after 3 cycles (Fig. S1 and Table S1). The SEM results show that after adsorption-desorption cycle (Fig. S1), the surface morphology of the basic material of MCM did not change, but the elemental analysis results showed that the number of N content on the MCM appeared to decrease sharply, and O content also appeared a decline (Table S1). This result was confirmed the N and O group was damaged or replaced by other ions, and the N-containing and O-containing functional groups on anion adsorption had a good effect; therefore, the decline in N and O functional groups could be the cause of the material performance degradation during the adsorption-desorption cycle experiments, possibly due to the destruction of N and O groups in the NaOH solution.

3.4. Competitive adsorption simulation

The phosphate concentration was set at 100 mg/L, the amount of the MCM was set at 0.4 g/L, and SO_4^{2-}, CO_3^{2-}, Cl^-, and Na^+ at 50 mg/L were added to test the selective adsorption of phosphate on the MCM. The simulation results show that among the four ions, Na^+ and Cl^- had almost no effect on the adsorption of phosphate onto the MCM, and CO_3^{2-} and SO_4^{2-} had a little influence on the adsorption of phosphate due to the properties of CO_3^{2-}, SO_4^{2-} and PO_4^{3-} or HPO_4^{2-} and their morphological similarity (Fig. 8a). However, these ions only reduced the performance by approximately 6–7%. By mixing the four ions and phosphate, it was found that the adsorption amount only decreased by 9.5%, which confirmed that the MCM had a high selective adsorption ability for phosphate and was an excellent material for phosphate removal.

3.5. Phosphate removal from actual water bodies

To judge whether the adsorbent can be applied in practice, it is necessary to test its phosphate removal effect in real water. The removal effect of MCM on phosphate in five kinds of real water was tested: deionized water, tap water, artificial lake at Northwest A&F University (China), Wei River (The largest tributary of the Yellow River in China) and rainwater. In order to compare the properties of the materials in different water bodies, the concentration of phosphate in five water bodies was adjusted to 1000 μg/L, and the amount of adsorbent is 0.4 g/L. The

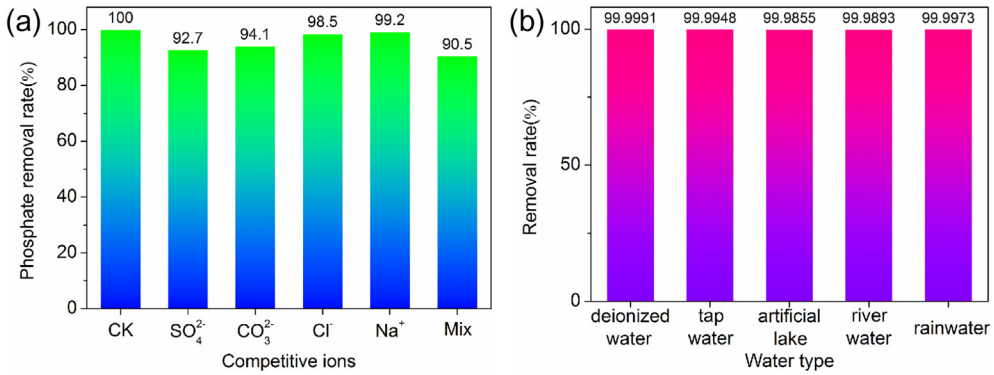

Fig. 8. Effects of competing ions and different water bodies on MCM adsorption of phosphate: (a) is competitive adsorption simulation diagram and (b) is phosphate removal effect in actual water bodies.

experimental results showed that the removal rate of phosphate by MCM in five kinds of water was more than 99.98% (Fig. 8b), and the residual concentration was far below the 10 μg/L suggested by USEPA (Shi et al., 2019). This indicates that MCM has a good effect on phosphate removal in actual water bodies and can improve the eutrophication problem in water bodies.

3.6. Adsorption mechanism

It is of great significance to understand the mechanism of adsorption phosphate by MCM. According to the results of kinetics model and adsorption diffusion model, the adsorption of phosphate on MCM is mostly chemical action, and are also some physical interaction (part of Section 3.2.2). In this study, C, N, O and P elements on MCM after adsorption were tested by SEM-EDX mapping, and it was found that P, O and N elements were similar in distribution on MCM, confirming that O and N groups were involved in MCM adsorption process of phosphate (Fig. S2). Meanwhile, Zeta potential analysis showed that the pH_{pzc} of MCM is about 4.7 (Fig. 5c). When the pH is less than 4.7, the amino group will be protonated, N element mainly exists in the form of $—NH_3^+$/$—NHR^+$/$—NR_2^+$ through electrostatic interaction to adsorb phosphate (mainly anions); when the pH is greater than 4.7, the N element mainly exists in the form of —NH— and $—NH_2$— to adsorb phosphate through ion complexation (Zhao et al., 2020). In addition, FTIR analysis showed that there was a large amount of —OH on MCM, and —OH could adsorb phosphate through hydrogen bonding and electrostatic interaction (Fig. S3). Therefore, there are four main adsorption mechanisms of MCM for phosphate: physical adsorption, electrostatic interaction, ion complexation and hydrogen bonding (Fig. 9).

4. Conclusion

At present, the cost of phosphate adsorbents is high, the adsorption performance is low and it is difficult to recycle. In this study, a novel MCM that can be reused for many times was synthesized for phosphate removal in wastewater. The adsorption experiments indicate that the MCM has a high adsorption ability for phosphate in a wide range of pH (1.5–10). The adsorption of phosphate by MCM follow the pseudo-second-order kinetic and Langmuir model, which indicate the adsorption is mono-layer adsorption and mainly chemical adsorption process. The q_{max} of MCM for phosphate was 123.73 mg/g (318 K), which higher than that of most materials. The thermodynamic results indicated that the adsorption of phosphate by MCM was spontaneous and endothermic. The main mechanisms for phosphate adsorption by MCM are physical adsorption, electrostatic attraction, complexation and hydrogen bonding. Competitive adsorption simulations and 20 regenerative cycles indicated that MCM had a high selectivity and a good regeneration performance for phosphate adsorption. In addition, it was found that the decrease of oxygen and nitrogen functional groups was the main reason for the degradation of the regeneration performance of the

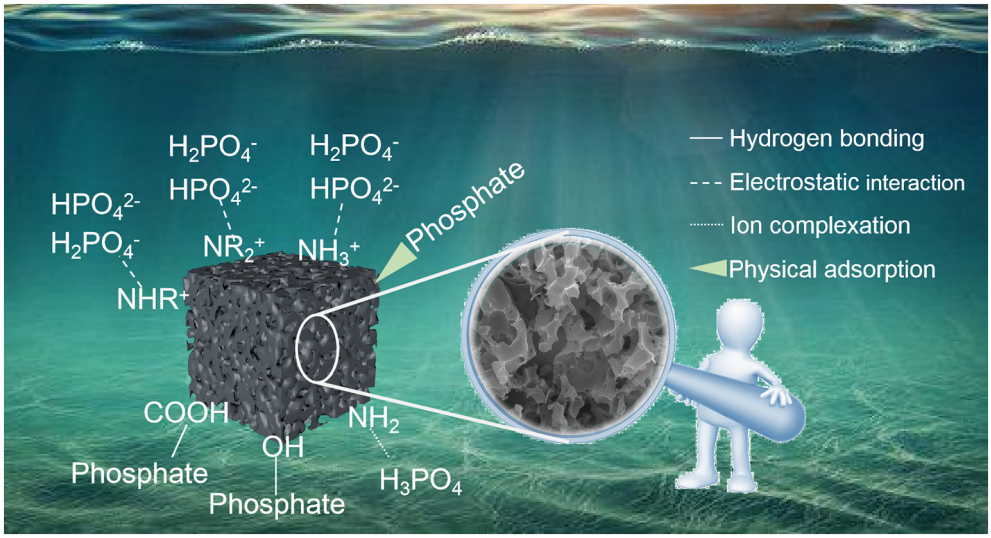

Fig. 9. The schematic diagram of MCM adsorption mechanism of phosphate.

materials. Phosphate removal experiments were carried out in deionized water, tap water, artificial lake, rainwater and river water (phosphate concentration 1000 μg/L), and the results showed that the removal rates were all higher than 99.98%, which confirmed that MCM could be applied to phosphate removal in actual water bodies. In conclusion, MCM prepared in this study can efficiently and selectively remove phosphate and can be reused for many times, which can effectively improve water eutrophication.

CRediT authorship contribution statement

Hongxu Liang: Conceptualization, Data curation, Formal analysis, Validation, Writing – original draft. **Hongwei Zhang:** Formal analysis, Investigation, Methodology. **Qiang Wang:** Investigation, Methodology, Validation. **Chenyang Xu:** Formal analysis, Methodology. **Zengchao Geng:** Funding acquisition, Resources, Project administration, Supervision, Writing – review & editing. **Diao She:** Funding acquisition, Resources, Supervision, Writing – review & editing. **Xuguang Du:** Formal analysis.

Declaration of competing interest

The authors declare that they have no known competing financial interests or personal relationships that could have appeared to influence the work reported in this paper.

Acknowledgments

This work was supported by the Ministry of Agriculture and Rural Affairs of the People's Republic of China (K3120217004), National Natural Science Foundation of China (31772390), STS Network Plan (KFJ-STS-QYZD-177), and the West Light Foundation of the CAS (XAB2018A05).

Appendix A. Supplementary data

Supplementary data to this article can be found online at https://doi.org/10.1016/j.scitotenv.2021.148452.

References

Acelas, N.Y., Martin, B.D., López, Diana, Jefferson, B., 2015. Selective removal of phosphate from wastewater using hydrated metal oxides dispersed within anionic exchange media. Chemosphere 119, 1353–1360.

Bacelo, H., Pintor, A.M.A., Santos, S.C.R., Boaventura, R.A.R., Botelho, C.M.S., 2020. Performance and prospects of different adsorbents for phosphorus uptake and recovery from water. Chem. Eng. J. 381, 122566.

Bhatti, Z.A., Qureshi, K., Maitlo, G., Ahmed, S., 2020. Study of PAN fiber and iron ore adsorbents for arsenic removal. Civil Eng. J. 6, 548–562.

Buaisha, M., Balku, S., Yaman, Ş.O., 2020. Heavy metal removal investigation in conventional activated sludge systems. Civ. Eng. J. 6, 470–477.

Bui, T.H., Hong, S.P., Kim, C., Yoon, J., 2021. Performance analysis of hydrated Zr(IV) oxide nanoparticle-impregnated anion exchange resin for selective phosphate removal. J. Colloid Interface Sci. 586, 741–747.

Carpenter, S.R., 2008. Phosphorus control is critical to mitigating eutrophication. P. Natl. Acad. Sci. U. S. A. 105, 11039–11040.

Carvalho, L., McDonald, C., Hoyos, C.D., Mischke, U., Phillips, G., Borics, G., Poikane, S., Skjelbred, B., Lyche Solheim, A., Van Wichelen, J., Cardoso, A.C., 2013. Sustaining recreational quality of European lakes: minimizing the health risks from algal blooms through phosphorus control. J. Appl. Ecol. 50, 315–323.

Cui, X., Dai, X., Khan, K.Y., Li, T., Yang, X., He, Z., 2016. Removal of phosphate from aqueous solution using magnesium-alginate/chitosan modified biochar microspheres derived from *Thalia dealbata*. Bioresour. Technol. 218, 1123–1132.

Cui, Q., Xu, J., Wang, W., Tan, L., Zheng, J., 2020. Phosphorus recovery by coreshell γ-Al2O3/Fe3O4 biochar composite from aqueous phosphate solutions. Sci. Total Environ. 729, 138892.

Deng, W., Tang, S., Zhou, X., Liu, Y., Luo, J., 2020. Honeycomb-like structure-tunable chitosan-based porous carbon microspheres for methylene blue efficient removal. Carbohydr. Polym. 247, 116736.

Fastner, J., Abella, S., Litt, A., Morabito, G., Matthews, D., Phillips, M.G., Chorus, I., 2015. Combating cyanobacterial proliferation by avoiding or treating inflflows with high P load experiences from eight case studies. Aquat. Ecol. https://doi.org/10.1007/s10452-015-9558-8.

Feng, Y., Lu, H., Liu, Y., Xue, L., Dionysiou, D.D., Yang, L., Xing, B., 2017. Nano-cerium oxide functionalized biochar for phosphate retention: preparation, optimization and rice paddy application. Chemosphere 185, 816–825.

Galvez-Cloutier, R., Saminathan, S.K., Boillot, C., Triffaut-Bouchet, G., Bourget, A., Soumis-Dugas, G., 2012. An evaluation of several in-lake restoration techniques to improve the water quality problem (eutrophication) of Saint-Augustin Lake, Quebec, Canada. Environ. Manag. 49, 1037–1053.

Gupta, K., Ghosh, U.C., 2009. Arsenic removal using hydrous nanostructure iron(III)-titanium(IV) binary mixed oxide from aqueous solution. J. Hazard. Mater. 161, 884–892.

Haddad, K., Jellali, S., Jeguirim, M., Trabelsi, A.B.H., Limousy, L., 2018. Investigations on phosphorus recovery from aqueous solutions by biochars derived from magnesium-pretreated cypress sawdust. J. Environ. Manag. 216, 305–314.

Hashim, K.S., Al Khaddar, R., Jasim, N., Shaw, A., Phipps, D., Kot, P., Pedrola, M.O., Alattabi, A.W., Abdulredha, M., Alawsh, R., 2019. Electrocoagulation as a green technology for phosphate removal from river water. Sep. Purif. Technol. 210, 135–144.

Huang, W.Y., Li, D., Liu, Z.Q., Tao, Q., Zhu, Y., Yang, J., Zhang, Y.M., 2014. Kinetics, isotherm, thermodynamic, and adsorption mechanism studies of La (OH)3-modified exfoliated vermiculites as highly efficient phosphate adsorbents. Chem. Eng. J. 236, 191–201.

Inagaki, M., Toyoda, M., Soneda, Y., Morishita, T., 2018. Nitrogen-doped carbon materials. Carbon 132, 104–140.

Jian, M.P., Liu, B., Zhang, G.S., Liu, R.P., Zhang, X.W., 2015. Adsorptive removal of arsenic from aqueous solution by zeolitic imidazolate framework-8 (ZIF-8) nanoparticles. Colloids Surf. A Physicochem. Eng. Aspects 465, 67–76.

Ketelle, B.H., Boyd, G.E., 1947. The exchange adsorption of ions from aqueous solutions by organic zeolites. IV. The separation of the yttrium group rare earths1. J. Am. Chem. Soc. 69, 2800–2812.

Klammsteiner, T., Turan, V., Fernandez-Delgado Juarez, M., Oberegger, S., Insam, H., 2020. Suitability of black soldier fly frass as soil amendment and implication for organic waste hygienization. Agronomy 10, 1578.

Li, J., Li, B., Huang, H., Lv, X., Zhao, N., Guo, G., et al., 2019. Removal of phosphate from aqueous solution by dolomite-modifified biochar derived from urban dewatered sewage sludge. Sci. Total Environ. 687, 460–469.

Liang, Q.W., Geng, J.J., Luo, H.J., Fang, W., Yin, Y.W., 2017. Fast and selective removal of Cr (VI) from aqueous solutions by a novel magnetic Cr (VI) ion-imprinted polymer. J. Mol. Liq. 248, 767–774.

Liang, Q.W., Luo, H.J., Geng, J.J., Chen, J.D., 2018. Facile one-pot preparation of nitrogendoped ultra-light graphene oxide aerogel and its prominent adsorption performance of Cr (VI). Chem. Eng. J. 338, 62–71.

Liang, H.X., Song, B., Peng, P., Jiao, G.J., Yan, X., She, D., 2019. Preparation of threedimensional honeycomb carbon materials and their adsorption of Cr(VI). Chem. Eng. J. 367, 9–16.

Liang, H.X., Sun, R.R., Song, B., Sun, Q.Q., Peng, P., She, D., 2020. Preparation of nitrogen-doped porous carbon material by a hydrothermal-activation two-step method and its high-efficiency adsorption of Cr(VI). J. Hazard. Mater. 387, 121987.

Liang, H.X., Zhang, H.W., Zhao, P.Y., Zhao, X.K., Sun, H.W., Geng, Z.C., She, D., 2021. Synthesis of a novel three-dimensional porous carbon material and its highly selective Cr (VI) removal in wastewater. J. Clean. Prod. 306, 127204.

Liu, J., Zhou, Q., Chen, J., Zhang, L., Chang, N., 2013. Phosphate adsorption on hydroxyl-iron-lanthanum doped activated carbon fiber. Chem. Eng. J. 215–216, 859–867.

Liu, S.W., Wang, X.B., Zhao, H.J., Cai, W.P., 2015. Micro/nano-scaled carbon spheres based on hydrothermal carbonization of agarose. Colloids Surf. A Physicochem. Eng. Asp. 484, 386–393.

Liu, T., Chen, X., Wang, X., Zheng, S., Yang, L., 2018. Highly effective wastewater phosphorus removal by phosphorus accumulating organism combined with magnetic sorbent MFC@La(OH) 3. Chem. Eng. J. 335, 443–449.

Liu, T., Zheng, S., Yang, L., 2019a. Magnetic zirconium-based metal-organic frameworks for selective phosphate adsorption from water. J. Colloid Interface Sci. 552, 134–141.

Liu, R., Chi, L., Wang, X., Wang, Y., Sui, Y., Xie, T., Arandiyan, H., 2019b. Effective and selective adsorption of phosphate from aqueous solution via trivalent-metals-based amino MIL-101 MOFs. Chem. Eng. J. 357, 159–168.

Liu, M., Li, S., Tang, N., Wang, Y., Yang, X., Wang, S., 2020. Highly efficient capture of phosphate from water via cerium-doped metal-organic frameworks. J. Clean. Prod. 265, 121782.

Meshkat, S.S., Nezhad, M.N., Bazmi, M.R., 2019. Investigation of carmine dye removal by green chitin nanowhiskers adsorbent. Emerg. Sci. J. 3, 187–194.

Naeem, I., Masood, N., Turan, V., Iqbal, M., 2021. Prospective usage of magnesium potassium phosphate cement combined with Bougainvillea alba derived biochar to reduce Pb bioavailability in soil and its uptake by *Spinacia oleracea* L. Ecotoxicol. Environ. Saf. 208, 111723.

Norouzi, S., Heidari, M., Alipour, V., Rahmanian, O., Fazlzadeh, M., Mohammadimoghadam, F., Nourmoradi, H., Goudarzi, B., Dindarloo, K., 2018. Preparation, characterization and Cr (VI) adsorption evaluation of NaOH-activated carbon produced from Date Press Cake; an agro-industrial waste. Bioresour. Technol. 258, 48–56.

Oginni, O., Singh, K., 2021. Effect of carbonization temperature on fuel and caffeine adsorption characteristics of white pine and Norway spruce needle derived biochars. Ind. Crop. Prod. 162, 113261.

Okpalugo, T.I.T., Papakonstantinou, P., Murphy, H., McLaughlin, J., Brown, N.M.D., 2005. High resolution XPS characterization of chemical functionalised MWCNTs and SWCNTs. Carbon 43, 153–161.

Rasool, B., Ramzani, P.M.A., Zubair, M., Khan, M.A., Lewińska, K., Turan, V., Iqbal, M., 2021. Impacts of oxalic acid-activated phosphate rock and root-induced changes on Pb bioavailability in the rhizosphere and its distribution in mung bean plant. Environ. Pollut. 280, 116903.

Saravanan, A., Karishma, S., Kumar, P.S., Varjani, S., Reshma, B., 2021. Simultaneous removal of Cu(II) and reactive green 6 dye from wastewater using immobilized mixed fungal biomass and its recovery. Chemosphere 271, 129519.

Shahbaz, A.K., Adnan Ramzani, P.M., Saeed, R., Turan, V., Iqbal, Muhammad, Lewińska, K., Abbas, F., Saqib, M., Tauqeer, H.M., Iqbal, Mutahar, Fatima, M., Rahman, M., 2019. Effects of biochar and zeolite soil amendments with foliar proline spray on nickel immobilization, nutritional quality and nickel concentrations in wheat. Ecotoxicol. Environ. Saf. 173, 182–191.

Shan, S., Zhang, T., Wang, W., Liu, D., Shi, W., Cui, F., 2021. Magnetite/hydrated cerium(III) carbonate for efficient phosphate elimination from aqueous solutions and the mechanistic investigation. Chem. Eng. J. 425, 128894.

Shi, W., Fu, Y., Jiang, W., Ye, Y., Kang, J., Liu, D., Ren, Y., Li, D., Luo, C., Xu, Z., 2019. Enhanced phosphate removal by zeolite loaded with Mg–Al–La ternary (hydr)oxides from aqueous solutions: performance and mechanism. Chem. Eng. J. 357, 33–44.

Sonmez, O., Turan, V., Kaya, C., 2016. The effects of sulfur, cattle, and poultry manure € addition on soil phosphorus. Turk. J. Agric. For. 40 (4), 536–541.

Sun, X., Li, Y., 2004. Colloidal carbon spheres and their core/shell structures with noblemetal nanoparticles. Angew. Chem. 116, 607–611.

Tong, X., Chen, Z.H., Zhuo, H., Hu, Y.J., Jing, S.S., Liu, J.C., Zhong, L.X., 2019. Tailoring the physicochemical properties of chitosan-derived N-doped carbon by controlling hydrothermal carbonization time for high-performance supercapacitor applicationle. Carbohydr. Polym. 207, 764–774.

Turan, V., 2019. Confident performance of chitosan and pistachio shell biochar on reducing Ni bioavailability in soil and plant plus improved the soil enzymatic activities, antioxidant defense system and nutritional quality of lettuce. Ecotoxicol. Environ. Saf. 183, 109594.

Turan, V., 2020. Potential of pistachio shell biochar and dicalcium phosphate combination to reduce Pb speciation in spinach, improved soil enzymatic activities, plant nutritional quality, and antioxidant defense system. Chemosphere 245, 125611.

Turan, V., Khan, S.A., Ur-Rahman, M., Iqbal, M., Ramzani, P.M.A., Fatima, M., 2018a. Promoting the productivity and quality of brinjal aligned with heavy metals immobilization in a wastewater irrigated heavy metal polluted soil with biochar and chitosan. Ecotoxicol. Environ. Saf. 161, 409–419.

Turan, V., Ramzani, P.M.A., Ali, Q., Abbas, F., Iqbal, M., Irum, A., Khan, W.U.D., 2018b. Alleviation of nickel toxicity and an improvement in zinc bioavailability in sunflflower seed with chitosan and biochar application in pH adjusted nickel contaminated soil. Arch. Agron. Soil Sci. 64 (8), 1053–1067.

Turan, V., Schroder, P., Bilen, S., Insam, H., Juárez, M.F.-D., 2019. Co-inoculation effect of rhizobium and *Achillea millefolium* L. oil extracts on growth of common bean (*Phaseolus vulgaris* L.) and soil microbial-chemical properties. Sci. Rep. 9, 15178.

Unuabonah, E.I., Agunbiade, F.O., Alfred, M.O., Adewumi, T.A., Okoli, C.P., Omorogie, M.O., Akanbi, M.O., Ofomaja, A.E., Taubert, A., 2017. Facile synthesis of new amino-functionalized agrogenic hybrid composite clay adsorbents for phosphate capture and recovery from water. J. Clean. Prod. 164, 652–663.

Vikrant, K., Kim, K.-H., Ok, Y.S., Tsang, D.C.W., Tsang, Y.F., Giri, B.S., Singh, R.S., 2018. Engineered/designer biochar for the removal of phosphate in water and wastewater. Sci. Total Environ. 616–617, 1242–1260.

Wang, Y., Yu, F., Zhu, M., Ma, C., Zhao, D., Wang, C.A., Zhou, Dai, B., Ji, J., Guo, X., 2018. N-doping of plasma exfoliated graphene oxide via dielectric barrier discharge plasma treatment for the oxygen reduction reaction. J. Mater. Chem. A Mater. Energy Sustain. 6, 2011–2017.

Wang, B., Ma, Y., Lee, X., Wu, P., Chen, M., 2020. Environmental-friendly coal gangue-biochar composites reclaiming phosphate from water as a slow-release fertilizer. Sci. Total Environ. 758, 143664.

Wu, Z.B., Zhong, H., Yuan, X.Z., Wang, H., Wang, L.L., Cheng, X.H., Zeng, G.M., Wu, Y., 2014. Adsorptive removal of methylene blue by rhamnolipid-functionalized graphene oxide from wastewater. Water Res. 67, 330–344.

Xiong, W., Tong, J., Yang, Z., Zeng, G., Zhou, Y., Wang, D., Song, P., Xu, R., Zhang, C., Cheng, M., 2017. Adsorption of phosphate from aqueous solution using iron-zirconium modified activated carbon nanofiber: performance and mechanism. J. Colloid Interface Sci. 493, 17–23.

Yin, Q., Ren, H., Wang, R., Zhao, Z., 2018. Evaluation of nitrate and phosphate adsorption on Al-modifiified biochar: inflfluence of Al content. Sci. Total Environ. 631–632, 895–903.

Zazycki, M.A., Godinho, M., Perondi, D., Foletto, E.L., Collazzo, G.C., Dotto, G.L., 2018. New biochar from pecan nutshells as an alternative adsorbent for removing reactive red 141 from aqueous solutions. J. Clean. Prod. 171, 57–65.

Zhang, M., Gao, B., Yao, Y., Inyang, M., 2013. Phosphate removal ability of biochar/MgAl-LDH ultra-fine composites prepared by liquid-phase deposition. Chemosphere 92, 1042–1047.

Zhang, X., Lin, X., He, Y., Chen, Y., Zhou, J., Luo, X., 2018. Adsorption of phosphorus from slaughterhouse wastewater by carboxymethyl konjac glucomannan loaded with lanthanum. Int. J. Biol. Macromol. 119, 105–115.

Zhang, H., Elskens, M., Chen, G., Chou, L., 2019. Phosphate adsorption on hydrous ferric oxide (hfo) at different salinities and pHs. Chemosphere 225, 352–359.

Zhao, Y., Shan, X., An, Q., Xiao, Z., Zhai, S., 2020. Interfacial integration of zirconium components with amino-modified lignin for selective and efficient phosphate capture. Chem. Eng. J. 398, 125561.

Zong, E.M., Wei, D., Wan, H.Q., Zheng, S.R., Xu, Z.Y., Zhu, D.Q., 2013. Adsorptive removal of phosphate ionsfrom aqueous solution using zirconia-functionalized graphite oxide. Chem. Eng. J. 221, 193–203.

Zong, E., Huang, G., Liu, X., Lei, W., Jiang, S., Ma, Z., Wang, J., Song, P., 2018. Lignin-based nano-adsorbent for superfast and highly selective removal of phosphate. J. Mater. Chem. A 6, 9971–9983.

Zubair, M., Ramzani, P.M.A., Rasool, B., Khan, M.A., Ur-Rahman, M., Akhtar, I., Turan, V., Tauqeer, H.M., Farhad, M., Khan, S.A., Iqbal, J., Iqbal, M., 2021. Efficacy of chitosancoated textile waste biochar applied to Cd-polluted soil for reducing Cd mobility in soil and its distribution in moringa (*Moringa oleifera* L.). J. Environ. Manag. 284, 112047.